

1 **Development of ZrO₂-chitosan-hydroxyapatite nanocomposite films from Fish bone meal**
2 **waste for biomedical applications**

3 Kunduru Sumila Reddy ¹, Randhi Uma Devi ^{2*}, Annapragada Ratnamala ²

4 ¹*School of Science, GITAM University, Vishakhapatnam - 5300452*

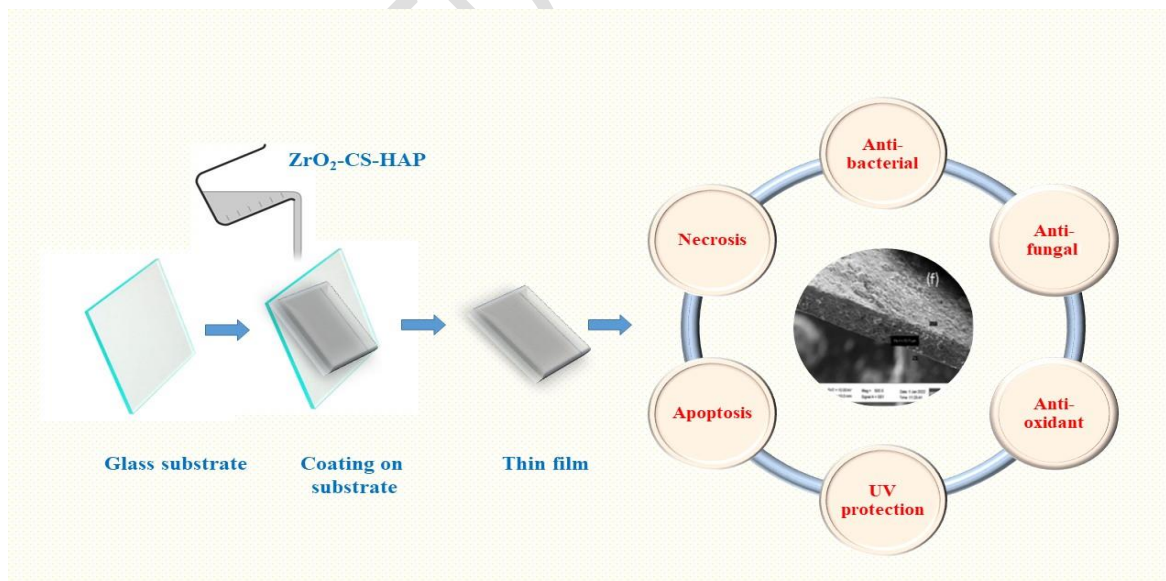
5 ²¹*School of Science, GITAM University, Hyderabad Campus, Telangana State, India-502329*
6 -----

7 **Abstract**

8 This study describes a simple way for making films from natural sources, which is relevant since
9 there is a rising demand for new materials that can make biocompatible films that are both
10 effective and economical for use in biomedical applications. Fish bone waste and chitosan, a
11 natural polymer used to manufacture thin films, are the sources of hydroxyapatites. The addition
12 of zirconia (ZrO₂) to the thin films created a new nanocomposite known as ZrO₂-Chitosan-
13 Hydroxyapatite (Zr-CS-HAP) films. These films demonstrated biocompatibility and have the
14 potential to be produced in huge quantities. The structural, morphological, and biological studies
15 were explored for possible biomedical applications like wound dressing, bone tissue
16 regeneration, etc. The films showed good anti-oxidant and UV-protecting properties.
17 Cytotoxicity of films by MTT test suggests that HeLa cell lines showed moderate to good
18 cytotoxicity and better cervical properties. The films tested for Apoptosis-Necrosis in HeLa cells
19 showed induced apoptosis of 52% and Necrosis of 21.3% in HeLa cells, similar to standard
20 control.

21
22 **Keywords:** Chitosan, Hydroxyapatite, Cytotoxicity, Anti-Microbial Susceptibility, Apoptosis,
23 Necrosis

24 Corresponding authors : urandhi@gitam.edu



25

26

27

29 **1 Introduction**

30 Bioceramic materials used for knee, femur, hip, teeth, and other biological implants are designed
31 to be highly absorbent and, in addition to their adequate load-bearing ability, can encourage the
32 formation of natural bone tissue on the surfaces of artificial joints (Mythili *et al.* 2015). The
33 creation of hybrid biomaterials with antibacterial, antifungal, anti-proliferative, and antioxidant
34 capabilities is crucial for promoting quicker and more effective healing. In order to achieve
35 superior orthopedic outcomes, an implant material must be mechanically and biologically sound
36 and pass a corrosion-resistant test (Cunha *et al.* 2020). Metallic bio implant materials are
37 essential in clinical applications because of their better mechanical qualities in physiological
38 conditions. Hydroxyapatite [$\text{Ca}_{10}[\text{PO}_4]_6[\text{OH}]_2$], a calcium /phosphate-based bio-ceramic (Komal
39 *et al.* 2020) chemically like an inorganic constituent of bone tissue, and is non inflammatory, non
40 immunogenic, biocompatible but also bioactive, has the ability to form a direct bond with living
41 tissue (Fathi *et al.* 2008). It promotes tissue growth and is used as a prosthetic implant and filler
42 material to replace damaged bones. Hydroxyapatite is promising for bone therapy, bone
43 replacement, bone repair material, and wound dressing material (Rinaudo, 2006). Although HAP
44 has a significant potential for wound healing because to its high biocompatibility and excellent
45 angiogenic activity, traditional HAP materials are not suitable for wound dressing due to their
46 high brittleness and poor mechanical qualities. However, the ability to add different dopants or
47 reinforcements to HAP improves its qualities and expands its applications (Lansdown, 2002).
48 Zirconium dioxide (ZrO_2) is a widely used material due to its excellent properties like
49 biocompatibility, excellent mechanical strength, elastic modulus equivalent to that of bones, low
50 stress, and high fracture toughness (Horti *et al.* 2020). Zirconia-based composite materials have
51 superior corrosion resistance, high hardness, fracture toughness, and less magnetic susceptibility,
52 making them useful for a variety of biomedical applications. One of the major components used
53 in biomedicine is chitosan (CS), obtained by deacetylation from chitin, a natural polysaccharide
54 found in crustacean shells. Chitosan has many biological properties, such as antibacterial,
55 nontoxic, and biodegradable. The degree of deacetylation (DDA) has a considerable impact on
56 the solubility of chitosan. Chitosan is soluble up to a pH of 9 when its DDA is less than 40%.
57 The Development and characterization of chitosan films were done to study the morphology and
58 physical, mechanical, and degradation properties (Yang *et al.* 2010).

59 **2 Methodology**

60 Local market fish bones are defatted and deproteinized. Crushed bone species cleaned after 2
61 hours in acetone and heated to 250°C for six hours while stirring in a highly concentrated 4N
62 sodium hydroxide solution with a 1:40 solid/liquid weight ratio. 20 g of bone powder in a
63 crucible is heated at 650°C @ 5°C for 6 h and 950°C for 6 hours (Barakat *et al.* 2008). A beaker
64 with 1M ammonium hydroxide contained the estimated amounts of ZrOCl_2 , a precursor to ZrO_2 ,
65 and bone powder to maintain pH 8. At 65–70°C, the mixture is stirred often. After washing and
66 drying overnight at 45° C, the solid is calcined at 700° C for an hour. With vigorous stirring,
67 Glacial acetic acid [1%v/v] dissolved chitosan at 25°C in 24 hours. Zr-HAP powder was added
68 in various amounts after dissolving. A 0.5 N NaOH solution and distilled water rinse neutralized
69 excess acetic acid. For film preparation, plasticizer glycerol was added and agitated at 40° C for
70 30 minutes to 60 mL. Glycerol as a plasticizer is added and swirled at 40° C for 30 minutes by
71 eliminating air bubbles and particles to make the film. The solution was cast and evaporated onto
72 a glass plate and dried for 72 h at 25 °C to form the film after 10 min of stirring at 40° C (Iline *et*

73 *al.* 2022). Zr concentrations and weight percents are in Table 1. The prepared films were
 74 characterized with XRD, SEM, FTIR (Srinivasan *et al.* 2018). A calibrated digital Vernier
 75 Calliper-gauge micrometer measures film thickness. Five locations are measured and averaged
 76 for each film. Film microstructure and quality may change with doping (Gao, 2004). Porosity
 77 was measured using a standard approach (Khorasani *et al.* 2019). Each film was weighed before
 78 and after 60 minutes in dry ethanol until saturated.

80 Table 1 Details of the weight percentages of the components used in the preparation of the film

S.No	Sample Name	Chitosan (deacetylated)	Percentage ZrO ₂ in Zr-HAP	Glycerol (mL)
1	Zr-CS-HAP-1 (Sample 1)	1% wt/v	1 wt/v % Zr on HAP	2.5
2	Zr-CS-HAP-2 (Sample 2)	1% wt/v	2 wt/v % Zr on HAP	3.5
3	Zr-CS-HAP-3 (Sample 3)	1% wt/v	3 wt/v % Zr on HAP	4.5
4	CS	1% wt/v	-	2.5
5	CS-HAP	1% wt/v	-	2.5

81
 82 To assess swelling and water-uptake (WU%), 25 × 25 mm films were submerged in 5 mL of
 83 saline solution (NaCl 0.9% w/v) adjusted to pH 6.6. WU at 120 minutes was calculated using
 84 weight differential %. Hydrated samples were submerged in solution and baked at 60 °C for 24
 85 hours to quantify erosion by weight. Erosion (E%) measures film weight loss in saline. For 24 h
 86 at 37 °C, the films were immersed in saline solution to measure disintegration and integrity.

87 Biological assessment

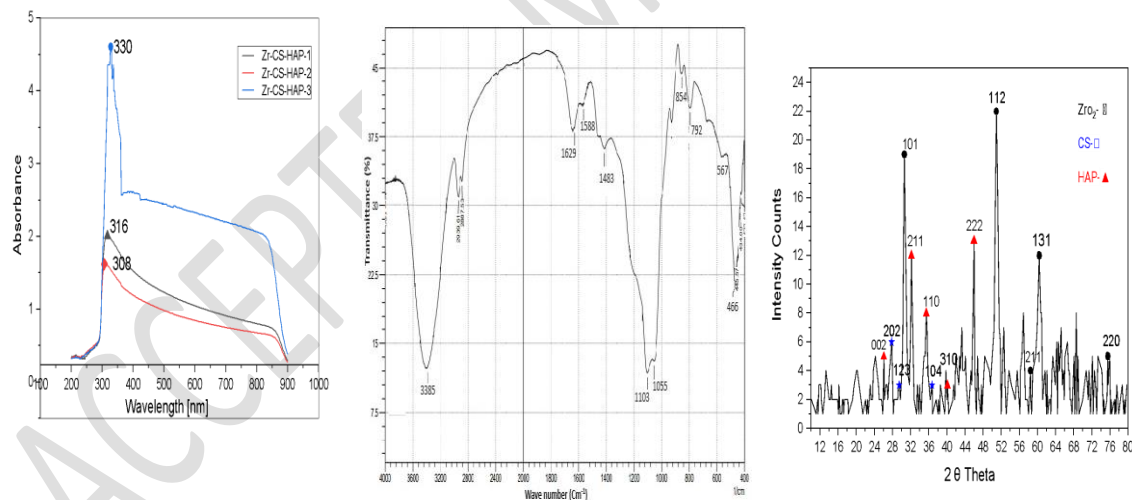
88 Human Cervix adenocarcinoma cell line HeLa is supplied from NCCS in Pune, India for film
 89 cytotoxicity. At 37°C with 5% CO₂ and 18–20% O₂, the cells were in DMEM with high glucose
 90 media, 10% FBS, and 1% antibiotic-antimycotic solution in a CO₂ incubator. Their subculture
 91 changed every two days. Colorimetric MTT cell proliferation assay used to measure cell
 92 proliferation and cytotoxicity (Gerlier and Thomasset, 1986). Antimicrobial susceptibility was
 93 tested on fungus (*Saccharomyces cerevisiae*), bacteria (*Escherichia coli*), and bacteria
 94 (*Staphylococcus aureus*). KIRBY Bauer Disc Diffusion showed a Zone of Inhibition for these
 95 species (Indumathi *et al.* 2019). To measure film antimicrobial activity, overnight liquid cultures
 96 of selected bacteria were diluted with 1 g L⁻¹ peptone and 8.5g L⁻¹ sodium chloride. UV light
 97 sterilized 1.3 cm CS and Zr-CS-HAP film discs for 10 minutes. To each disk in a sterile tube,
 98 200µl of liquid inoculum was added. The films were inoculated for 0, 2, 4, and 6 hours at 37 °C.
 99 Each tube was diluted with 1.8 mL peptone water (Tabassum *et al.* 2021). We cultivated 20 µl
 100 aliquots of each diluted solution on Muller Hinton Agar at 37 °C before counting colonies. A
 101 triple statistical analysis was performed on each experiment (Raphael and Meimandipor, 2017).
 102 Two samples of Zr-CS-HAP -2 and -3 were tested for antioxidant activity using DPPH free
 103 radical scavenging (McDonald *et al.* 2006). Apoptosis, Necrosis, and other types of cell death
 104 were characterised by the expression of phosphatidylserine on the cell surface, which is detected
 105 by using Annexin-V as a probe (Homburg *et al.* 1995). Thus, viable, early apoptotic, late
 106 apoptotic, and necrotic cells are represented by the populations Annex-V-/IP-, Annex-V+/IP-,
 107 Annex-V+/IP+, and Annex-V-/IP+, respectively (Obrien and Bolton, 1995). Following staining,

propidium iodide is represented by the pink stain and Annexin V by the green stain. The yellow tetrazolium dye MTT is reduced to formazan crystals by the MTT Assay test, which can be used to measure cytotoxicity and cell proliferation. To evaluate viability, the MTT test (3-[4,5-dimethyl-2-thiazol]-2,5-diphenyl-2H-tetrazolium bromide) was employed.

112

113 3 Results and discussion

114 XRD can determine Zr-CS-HAP's crystal structure and microstructure orientation using the thin
115 film detector. XRD patterns show strong crystallinity, ZrO₂, HAP, and Chitosan peaks. Zr-CS-
116 HAP diffraction peaks display the tetragonal phase of ZrO₂, coinciding with JCPDS card no. 89-
117 7710, with a significant peak at 2θ value 30.0°, corresponding to the (101) plane. HAP peaks at
118 2θ values of 26.0° (002), 32.2° (211), 40.1° (310), and 45.9° (222) match the hexagonal
119 structure of hydroxy apatite and JCPDS card no 09-0432 (Ashkezari *et al.* 2023). Chitosan had
120 low peaks at 2 theta 15, 20.0°, and 36.7°, as before (R palla *et al.* 2012). FTIR functional
121 groups of the composite film are presented in Figure 1. O-H stretching causes the spectrum's big
122 peak at 3385 cm⁻¹. Chitosan amine peaks at 1629 cm⁻¹ (Madeha and Ntanoyenkosi, 2024).
123 Peaks at 567, 1055, and 1566 cm⁻¹ (phosphate groups) indicate HAP (Panda *et al.* 2003).
124 Spectrum data at 854, 1,413, and 1,451 cm⁻¹ suggests carbonate ions. Also observed are Zr-O
125 stretching peaks at 466 and 434. The spectrum shows all ZrO₂, Chitosan, and HAP peaks. A
126 Labsphere UV-2000F ultraviolet transmittance tester measured a few films' UPF (Balraj *et al.*
127 2017). Figure 1 depicts Zr-CS-HAP UV-visible diffuse reflectance spectra with various zirconia
128 loadings. Figure shows absorption is concentrated at 308, 316, and 330 nm. Valence band to
129 conduction band transition may explain this. ZrO₂ nanosheets displayed no extrinsic states and a
130 high peak at 319 and 330 nm, according to literature. This suggested minor ZrO₂ nanosheet
131 surface defects (Fatemh and Mohammad, 2014).



132

133 Fig.6 UV-Vis DRS spectra, FTIR and XRD of Zr-CS-HAP thin films

134

135 A calibrated digital Vernier Calliper-gauge micrometer measures film thickness at five locations
136 for each film and calculates the average. Doping could alter film quality and microstructure.
137 Table 2 shows the weights of the films before and after 60 minutes in dry ethanol till saturated.
138 SEM micrographs of zirconia loaded on HAP films at different magnifications are shown in
139 Figure 2. Figures (2a) and (2b) show just chitosan film, (2c) and (2d) show rod-shaped CS-HAP
140 films, and (2e) and (2f) exhibit Zr-CS-HAP films. Homogeneous films with considerable ZrO₂

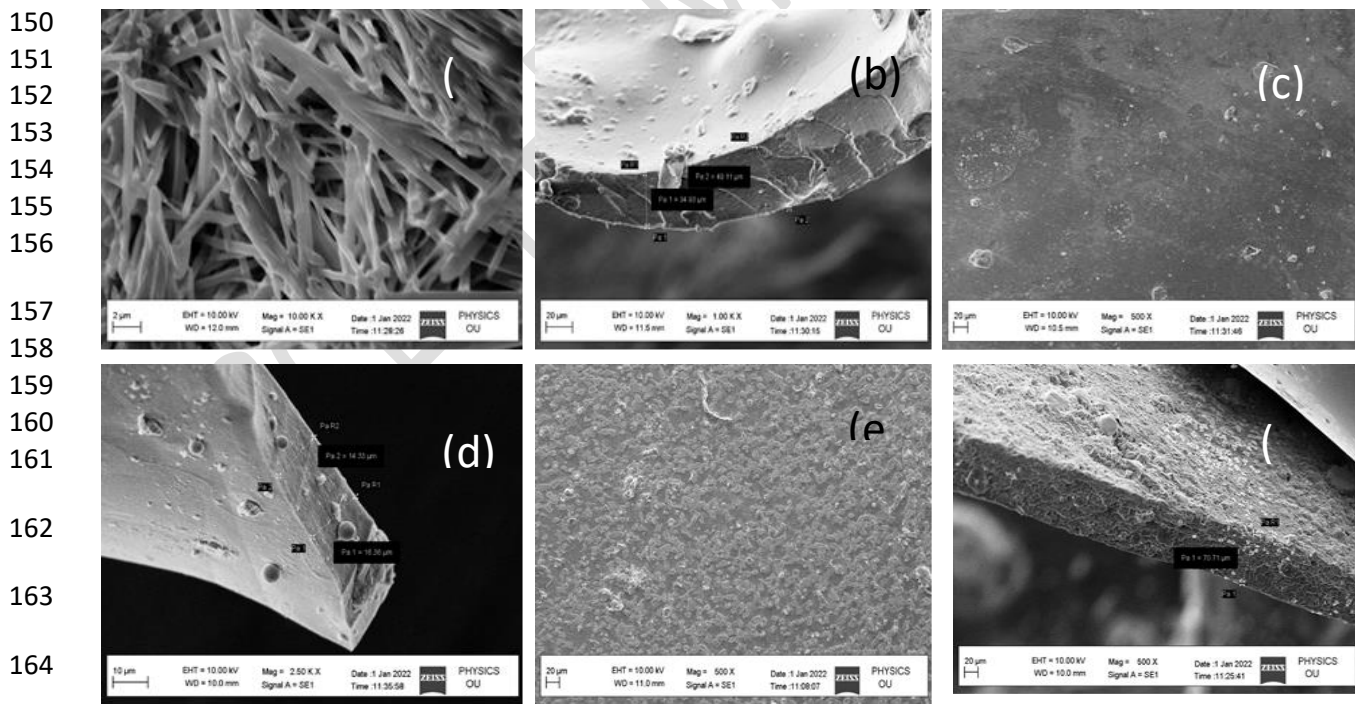
141 dispersion or nanofibers embedded in HAP films. SEM images reveal a film thickness of 14-49
 142 μm . These values match vernier caliper measurements. Figure 3 illustrates EDAX pattern and
 143 metal % at a given time.

144
 145

146 Table 2 Details of thickness, porosity, and UPF values critical wavelength and percentage
 147 transmittance

Sample Name	Thickness (mm)	Porosity (%)	Water uptake/time min^{-1} (%)	% Erosion	Water uptake %/min	UPF value	UPF rating	T UVA%	T UVA%
Zr-CS-HAP-1	0.025	26.61	1.6	50.0	2.9	153.38	excellent	0.57	2.25
Zr-CS-HAP-2	0.019	28.51	1.7	51.1	2.9	155.26	excellent	0.73	2.16
Zr-CS-HAP-3	0.020	29.78	2.2	52.3	2.5	140.15	excellent	0.31	2.21
CS	0.036	20.27	1.0	40	2.4	19.09	poor	0.68	2.27
CS-HAP	0.09	22.81	3.2	66	2.5	15.9	poor	0.65	2.31

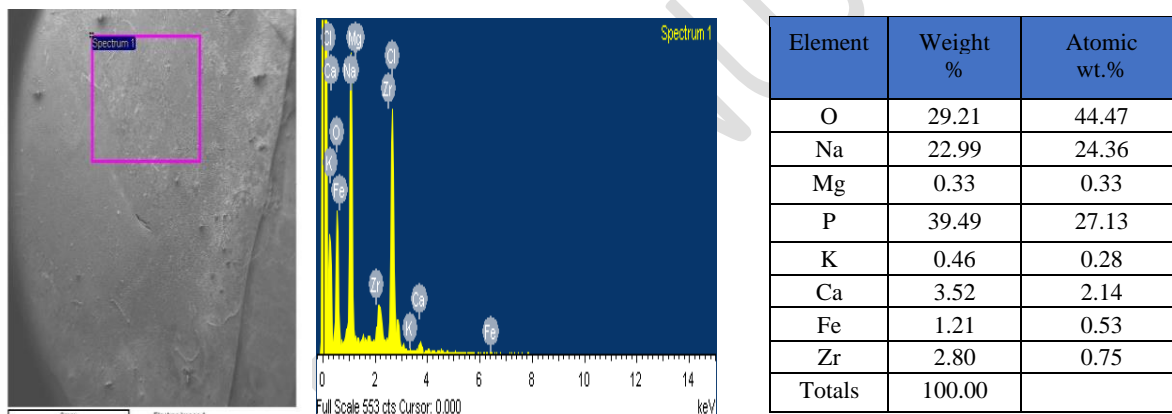
148
 149



166 Fig. 2 Scanning Electron Microscopes : (2a) & (2b) chitosan film, (2c) & (2d) CS-HAP, (2e) &
 167 (2f) Zr-CS-HAP

168 **MTT Assay**

169 Cytotoxicity should not be exhibited by biomaterials used in biological applications. Using an
 170 MTT assay, Zr-CS-HAP thin films were examined in vitro to determine the nontoxic
 171 concentration. This MTT (3-[4,5-dimethylthiazol-2-yl]-2,5 diphenyl tetrazolium bromide) assay,
 172 measures mitochondrial activity by watching how cells transform MTT into formazan crystals
 173 while they are still alive. The capacity of metabolically active cells to transform MTT into
 174 formazan crystals was assessed. Based on the observations in Statistical data of cell cytotoxicity
 175 study by MTT assay, it is suggesting that against HeLa cell lines, Test Compounds, namely Zr-
 176 CS-HAP-2 and Zr-CS-HAP-3 showing moderate cytotoxic potential properties with the IC₅₀
 177 Concentrations of 280µg/mL and 519µg/mL respectively. To demonstrate the mechanism of
 178 action of films on human cervical cancer cells, more research was conducted, including
 179 investigations on the cell cycle using PI staining, apoptosis using Annexin V/PI staining,
 180 apoptotic protein expressions such as Caspase 3,7,9, Bcl2, p53, and ROS.



181
 182 Fig.4 An EDAX Pattern of Zr-CS-HAP and a percentage of metal at a particular point
 183

184 It is acknowledged in the literature that CS is nontoxic, and the incorporation of HAP induces
 185 proliferative properties (Koopman *et al.* 1994). Moreover, the ZrO₂ was also reported to be
 186 bioinert, and these coatings were expected to improve the interaction with cells and tissues. The
 187 proliferation of the cells is due to the presence of calcium in hydroxyapatite. Calcium-sensing
 188 receptors trigger chemotaxis and proliferation in response to elevated extracellular calcium
 189 levels. In this regard, Zr-CS-HAP would be more beneficial because calcium can encourage
 190 development and proliferation through the mechanical strength of Zr-based ceramics.

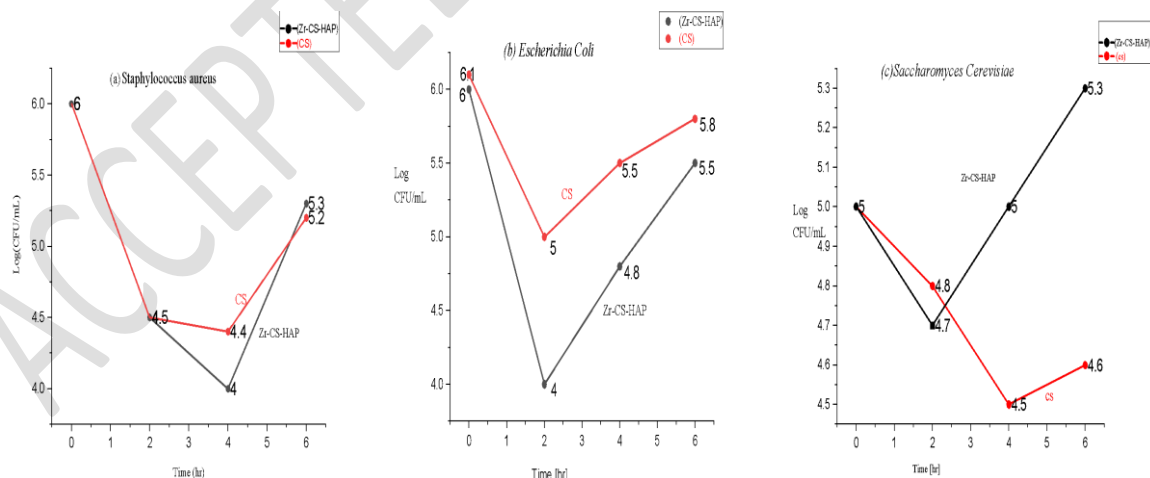
191
 192 **Anti-Microbial Susceptibility**

193 The antibacterial activity of Zr-CS-HAP films was evaluated against three different
 194 microbiological strains to see whether the powder's absorption into the film affected the behavior
 195 of Zirconium and HAP. The disc diffusion method and viable cell count assay measured the
 196 films' antibacterial and antifungal properties. The Zr-CS-HAP films repressed *Escherichia Coli*
 197 Gram Negative, *Staphylococcus aureus* Gram Positive, and *Saccharomyces cerevisiae*. Table 3
 198 lists the species and zone of inhibition. Films with less Zr-CS-HAP have smaller inhibition

199 zones. How well the inoculum kills germs depends on its concentration. Gram-positive bacteria
 200 show no influence from Zr-HAP in the film (Figure 4a). Staphylococcus aureus may be resistant
 201 to Chitosan films with a 1.5 log unit reduction. The regular Chitosan film and Zr-HAP film differ
 202 slightly yet considerably. Figure 4b targets Gram-negative *E. coli*. Both examples had two log
 203 units fewer live bacteria after two hours with UV-absorbing powder in their matrix, proving that
 204 the CS film is still effective against bacteria. A small shift occurred after 4 hours, and both
 205 samples reached 5 log CFU/mL after 6 hours. As with other antibacterial coatings, a modest
 206 uptick suggests weak microbial return. Although the bacterial population has grown, it is still
 207 modest. A *Saccharomyces cerevisiae* test on the CS film showed just a slight decrease in active
 208 microorganisms (Figure 4 c), ruling out considerable action. Live cells increased after 6 hours as
 209 the Zr-CS-HAP film grew. Fungal activity-promoting compounds may be released during
 210 incubation. The elements may be organic bits or molecules. Although the chemicals have been
 211 revealed in organism tests, the CS matrix's high antibacterial activity may have hidden their
 212 benefits. But additional investigation is needed. Overall, Zr-CS-HAP films have outstanding
 213 Gram-positive and Gram-negative antibacterial activity, peaking between 2 and 4 hours. Good
 214 wound dressings, Zr-CS-HAP films absorb UV radiation and are antibacterial.
 215
 216

Table 3 Details of the Microorganisms Used and Zone of Inhibition

S.No	Name of the Microorganisms	Antibiotic Disc	Zone of Inhibition
1	<i>Escherichia Coli</i>	Control Zr-CS-HAP -2 Zr-CS-HAP -3	Nil 1.5 mm 1.8 mm
2	<i>Staphylococcus aureus</i>	Control Zr-CS-HAP- 2 Zr-CS-HAP- 3	Nil 1.0 mm 1.0 mm
3	<i>Saccharomyces Cerevisiae</i>	Control Zr-CS-HAP- 2 Zr-CS-HAP- 3	Nil 1.0 mm 1.6 mm



217
 218 Figure 4 (a) Antimicrobial assay of simple chitosan (CS) and chitosan with Zr-HAP powder (Zr-
 219 CS-HAP-2) film capacity to inactivate Gram-positive bacteria
 220
 221

222 **DPPH RSA**

223 The CS-Zr-HAP films were studied for DPPH radical scavenging (RSA). The 2,2, diphenyl-
224 picrylhydrazyl (DPPH) technique has several medicinal and food-related uses. Antioxidant
225 activity of chemicals, especially phenolic compounds, can be evaluated using this approach. The
226 Spectrophotometer/ELISA reader's observations in the statistical results of the DPPH RSA study
227 show that the test compounds Zr-CS-HAP-2 and Zr-CS-HAP-3, inhibited DPPH RSA in a dose-
228 dependent manner with IC50 values of 663 µg/mL and 993µg/mL, respectively (Figure 5). The
229 standard control for the study was ascorbic acid. The measured DPPH radical scavenging
230 conclusions of the tested compounds (Zr-CS-HAP-3) reveal that they have significant dose-
231 dependent DPPH radical scavenging potency, while Zr-CS-HAP-2 and other samples have
232 moderate DPPH radical scavenging activity. Ascorbic acid & Zr-CS-HAP-2 both showed notable
233 DPPH radical scavenging efficacy in a dose-dependent manner (Ngugen *et al.* 2022).

234
235 Table 4 Comparative DPPH % inhibition in a dose-dependent manner
236

Concentration (µg/mL)	Zr-CS-HAP- 2	Zr-CS-HAP-3
DPPH alone	0	0
Ascorbic acid-10	44.45	44.45
62.5	4.45	0.13
125	8.58	2.22
250	13.44	6.95
500	30.87	10.40
1000	73.44	55.27

237
238 **Apoptosis and necrosis**

239 Annexin V/PI double labelling was used to quantify cell apoptosis and necrosis, and the results
240 are displayed in Fig. 5. When compared to the control group, the Zr-CS-HAP-2-treated cells
241 showed variable levels of necrosis instead of apoptosis. In late apoptosis or when the treatment
242 period was prolonged, the necrosis rates of the Zr-CS-HAP-2-treated cells rose from 21.35% to
243 43.11%. (A) % live, apoptosis and necrotic population observed in HeLa cells treated with
244 culture medium alone (Untreated), (B) Camptothecin and Test compound,(C) Zr-CS-HAP-
245 2, with 72.83µg/mL concentration (D) Quadrant plots showing the % of HeLa cells that are
246 alive, in apoptosis, and necrotic after being subjected to the amounts of Camptothecin (3.8
247 µM/mL), Test compound, Zr-CS-HAP-2, and culture media alone (Untreated), respectively.

248
249

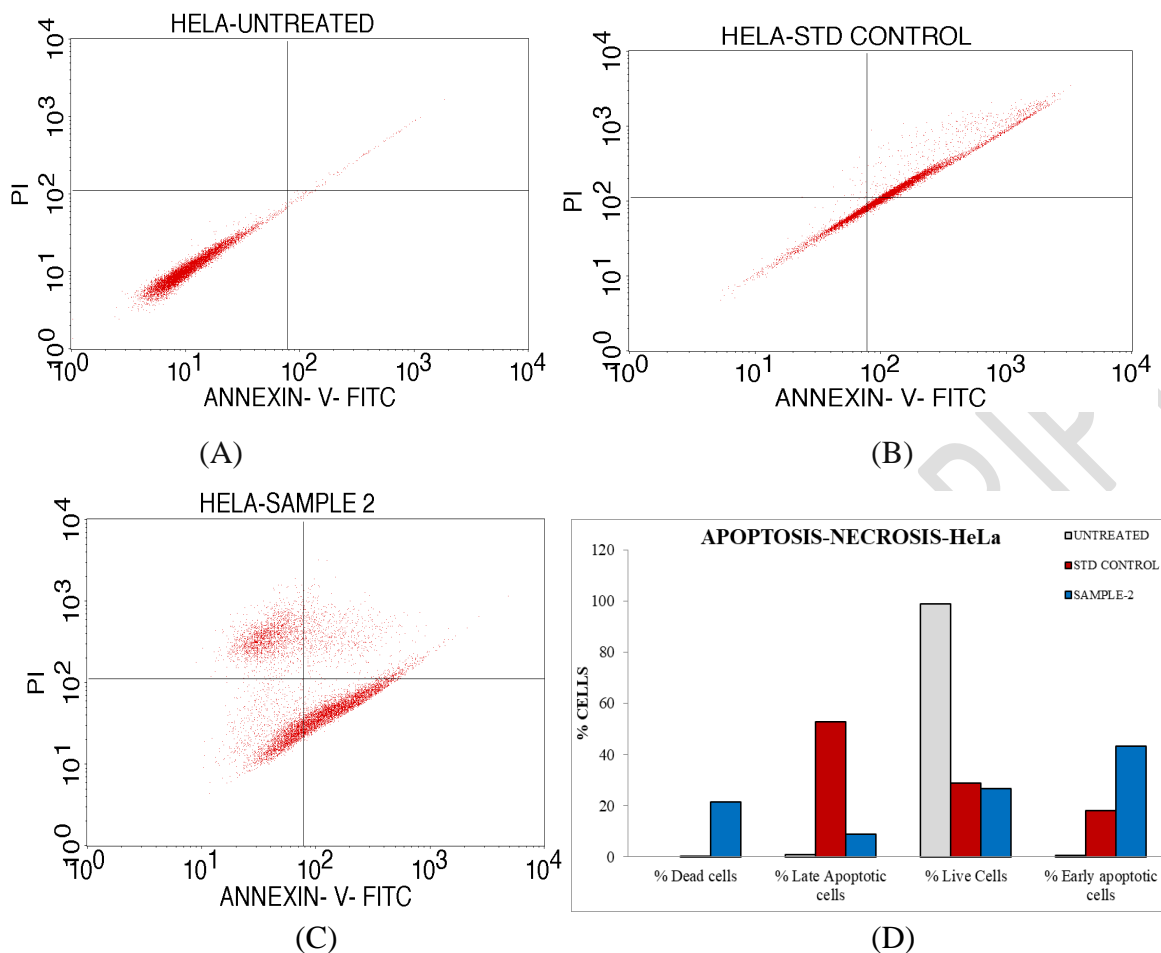


Figure 5 Apoptosis and Necrosis results

Table 5 Apoptosis and necrosis assay of cells exposed to Zr-CS-HAP-2 films

% population of cells	Necrosis	Late apoptosis	Live	Early apoptosis
Untreated	0	0.72	98.85	0.43
Camptothecin-3.8 μ M/mL	0.19	52.82	28.81	18.18
Zr-CS-HAP- 2 with 72.83 μ g/mL	21.35	8.93	26.61	43.11

The above graph and table clearly show that the study's Std control drug Camptothecin, the test substance Zr-CS-HAP-2, significantly increased the amount of apoptosis (52%) and necrosis (21.35%) in HeLa cells.

Conclusions

Chitosan, ZrO₂ HAP-based hybrid films were successfully prepared. The characteristics of these films indicate that they are suitable for biomedical applications like wound dressings because they help to reduce bacterial infections and bone tissue engineering applications. MTT assay,

266 DPPH, Apoptosis, and Necrosis studies also state that the Zr-CS-HAP-2 films have an impact
267 and possibility to explore in bone tissue engineering applications. Between two and four hours,
268 the Zr-CS-HAP films exhibit the highest level of antibacterial activity against both Gram-
269 positive and Gram-negative pathogens. The fungal organism *Saccharomyces Cerevisiae* has been
270 demonstrated to be mildly affected by Zr-CS-HAP film. Its bioactivity, biodegradability, and
271 biocompatibility make it highly beneficial in many scientific domains.

272

273 **References**

274 Ashkezari Shamim, Abtahi MaryamSadat ,SattariZahra. (2023), Antibiotic and inorganic
275 nanoparticles co-loaded into carboxymethyl chitosan-functionalized niosome: Synergistic
276 enhanced antibacterial and anti-biofilm activities, Journal of Drug Delivery Science and
277 Technology, 83, 104386. <https://doi.org/10.1016/j.jddst.2023.104386>

278 Balraj B, Arulmozhi M, Siva C, Krithikadevi R. (2017), Synthesis, characterization and
279 electrochemical analysis of hydrothermal synthesized AgO incorporated ZrO₂ nanostructures,
280 Journal of Materials Science: Materials in Electronics, 28(8), 5906- 5912.
281 <https://doi.org/10.1007/s10854-016-6264-9>

282 Barakat N.A.M, Khalil K. A, Sheikh F A. (2008), Physiochemical characterizations of
283 hydroxyapatite extracted from bovine bones by three different methods: Extraction of
284 biologically desirable HAP. Materials Science and Engineering: C, 28(8), 1381-
285 1387. <https://doi.org/10.1016/j.msec.2008.03.003>

286 Cunha C. S, Castro P. J, Sousa S. C, Pullar R. C. (2020), Films of chitosan and natural modified
287 hydroxyapatite as effective UV-protecting, biocompatible and antibacterial wound dressings.
288 International journal of biological macromolecules, 159, 1177-1185.
289 <https://doi.org/10.1016/j.ijbiomac.2020.05.077>

290 Fatemeh Davar, Mohammad Reza Loghman- Estarki. (2014), Synthesis and optical properties of
291 pure monoclinic zirconia nanosheets by a new precursor, Ceramics International, 40(6), 8427-
292 8433. <https://doi.org/10.1016/j.ceramint.2014.01.052>

293 Fathi M. H, Hanifi A, Mortazavi V, (2008), Preparation and bioactivity evaluation of bone-like
294 hydroxyapatite nanopowder. Journal of Materials Processing Technology, 202(1-3), 536-542.
295 <https://doi.org/10.1016/j.jmatprotec.2007.10.004>

296 Gao W. L, (2004), ZnO thin films produced by magnetron sputtering. 30(7), 1155-1159.
297 <https://doi.org/10.1016/j.ceramint.2003.12.197>

298 Gerlier D, Thomasset N, (1986), Use of MTT colorimetric assay to measure cell activation.
299 Journal of immunological methods, 94(1-2), 57-63. [https://doi.org/10.1016/0022-1759\(86\)90215-2](https://doi.org/10.1016/0022-1759(86)90215-2)

301 Homburg C.H, De Haas M., Von Dem Borne A.E. (1995), Human Neutrophils Lose Their
302 Surface Fc Gamma RIII and Acquire Annexin V Binding Sites During Apoptosis In Vitro.
303 Blood, 85(2), 532-540. <https://doi.org/10.1182/blood.V85.2.532.532>

304 Horti, N. C,Kamatagi M. D, Nataraj S. K, Wari M. N, Inamdar S. R. (2020), Structural and
305 optical properties of zirconium oxide (ZrO₂) nanoparticles: effect of calcination temperature,
306 Nano Express, 1(1), 010022. DOI: 10.1088/2632-959X/AB8684

307 Iline-Vul T, Kanovsky N, Yom-Tov D, Nadav-Tsubery M, Margel S, (2022), Design of silane-
308 based UV-absorbing thin coatings on polyethylene films,Colloids and Surfaces A:
309 Physicochemical and Engineering Aspects, 648,
310 129164. <https://doi.org/10.1016/j.colsurfa.2022.129164>

311 Indumathi M.P, Sarojini K.S, Raja Rajeswari G.R. (2019), Antimicrobial and biodegradable
312 chitosan/cellulose acetate phthalate/ZnO nano composite films with optimal oxygen permeability
313 and hydrophobicity for extending the shelf life of black grape fruits. *International Journal of*
314 *Biological Macromolecules*, 132, 1112-1120. <https://doi.org/10.1016/j.ijbiomac.2019.03.171>
315 Khorasani M. T, Joorabloo A, Adeli H, Mansoori-Moghadam Z, Moghaddam A. (2019), Design
316 and optimization of process parameters of polyvinyl (alcohol)/chitosan/nano zinc oxide
317 hydrogels as wound healing materials. *Carbohydrate Polymers*, 207, 542-554.
318 <https://doi.org/10.1016/j.carbpol.2018.12.021>
319 Komal Prasad Malla, Sagar Regmi, Achyut Nepal. (2020), Extraction and Characterization of
320 Novel Natural Hydroxyapatite Bioceramic by Thermal Decomposition of Waste Ostrich Bone.
321 *International Journal of Biomaterials*. ArticleID 1690178. <https://doi.org/10.1155/2020/1690178>
322 Koopman G, Reutelingsperger C.P, Kuijten G.A. (1994), Rapid Communication Annexin V for
323 flow cytometric detection of phosphatidylserine expression on B cell undergoing apoptosis.
324 *Blood* 84 (5), 1415-1420. <https://doi.org/10.1182/blood.V84.5.1415.1415>
325 Lansdown A.B.G. (2002), Calcium: a potential central regulator in wound healing in the skin.
326 *Wound repair and regeneration* 10 (5), 271–285. [https://doi.org/10.1046/j.1524-](https://doi.org/10.1046/j.1524-475X.2002.10502.x)
327 [475X.2002.10502.x](https://doi.org/10.1046/j.1524-475X.2002.10502.x)
328 MacDonald-Wicks L.K, Wood L.G, Garg M.L. (2006), Methodology for the determination of
329 biological antioxidant capacity in vitro: a review. *Journal of the Science of Food and Agriculture*,
330 86(13), 2046-2056. <https://doi.org/10.1002/jsfa.2603>
331 Madeha Al-Kelani ,Ntandoyenkosi Buthelezi. (2024), Advancements in medical research:
332 Exploring Fourier Transform Infrared (FTIR) spectroscopy for tissue, cell, and hair sample
333 analysis, *Skin Research and Technology* 2024, <https://doi.org/10.1111/srt.13733>
334 Mythili Prakasam, Janis Locs, Kristine Salma- Ancane. (2015), Fabrication, properties and
335 applications of dense hydroxyapatite: A review . *Journal of functional Biomaterials*, 6(4), 1099–
336 1140. <https://doi.org/10.3390/jfb6041099>
337 Nguyen Mai Thanh Thao, Huynh Van Tri, Tran Nguyen Gia Han. (2022), Measure the
338 ultraviolet protection factor (UPF) of Fabrics on UV-Vis spectrophotometer, *Journal of Science*
339 *Technology and Food* 22(3), 321-329.
340 O'Brien M C, W E. Bolton W E. (1995), Comparison of cell viability probes compatible with
341 fixation and permeabilization for combined surface and intracellular staining in flow cytometry.
342 *Journal of Quantitative cell science*, 19(3), 243-255. <https://doi.org/10.1002/cyto.990190308>
343 Panda R.N, Hsieh M.F, Chung R.J, Chin T.S. (2003), FTIR, XRD, SEM and solid state NMR
344 investigations of carbonate-containing hydroxyapatite nano-particles synthesized by hydroxide-
345 gel technique, *Journal of Physics and Chemistry of Solids*, 64(2), 193-
346 199. [https://doi.org/10.1016/S0022-3697\(02\)00257-3](https://doi.org/10.1016/S0022-3697(02)00257-3)
347 R. Pallela R , J Venkatesan J , Janapala V.R , Kim S.K. (2012), Bio physicochemical evaluation
348 of chitosan hydroxyapatite-marine sponge collagen composite for bone tissue engineering.
349 *Journal of Biomedical Materials Research Part A* :100A, 486–495.
350 <https://doi.org/10.1002/jbm.a.33292>
351 Raphaël K.J and Meimandipour A. (2017), Antimicrobial Activity of Chitosan Film Forming
352 Solution Enriched with Essential Oils; an in Vitro Assay. *Iranian Journal of Biotechnology*,
353 15(2), 111–119. <https://doi.org/10.15171/ijb.1360>
354 Rinaudo M. (2006), Chitin and chitosan: Properties and applications. *Progress in Polymer*
355 *Science*, 31(7), 603-632. <https://doi.org/10.1016/j.progpolymsci.2006.06.001>

356 Srinivasan H, Kanayairam V, Ravichandran R. (2018), Chitin and chitosan preparation from
357 shrimp shells *Penaeus monodon* and its human ovarian cancer cell line, PA-1, International
358 Journal of Biological Macromolecules, 107, 662-
359 667. <https://doi.org/10.1016/j.ijbiomac.2017.09.035>
360 Tabassum N, Kumar D, Verma D, Raghvendra A. Bohara, Singh M.P. (2021), Zirconium oxide
361 (ZrO_2) nanoparticles from antibacterial activity to cytotoxicity: A next Generation of
362 multifunctional nanoparticles, Materials Today Communications, 26, 102156.
363 <https://doi.org/10.1016/j.mtcomm.2021.102156>
364 Yang, Yajuan Liu, Changhua Wu, Haixia Li, Rui. (2010), Preparation and characterization of
365 films based on zirconium sulfophenyl phosphonate and chitosan, Carbohydrate research, 345(1),
366 148-153. DOI: 10.1016/J.CARRES.2009.10.012.

ACCEPTED MANUSCRIPT